Dyes and Pigments 170 (2019) 107556

Contents lists available at ScienceDirect

Dyes and Pigments

journal homepage: www.elsevier.com/locate/dyepig

Exceptional aggregation-induced emission from one totally planar molecule

Ying-Xue Yuan, Bai-Xing Wu, Jia-Bin Xiong, Hong-Chao Zhang, Ming Hu, Yan-Song Zheng*

Key Laboratory for Large-Format Battery Materials and System, Ministry of Education, School of Chemistry and Chemical Engineering, Huazhong University of Science and Technology, Wuhan, 430074, China

ARTICLE INFO

Keywords:
AIE
Planar molecule
Intramolecular charge transfer
Slipped π-π stacking
A-D-A triad

ABSTRACT

Planar molecules usually display aggregation-caused quenching (ACQ). Here, it was found that a completely planar organic compound, 5,7,12,14-tetraoxapentacene A-D-A triad with carbon-oxygen bonds, had no fluorescence in high polar solvents but emitted strong light in suspension and in solid state, showed typical AIE effect. One novel AIE mechanism was disclosed by molecular packing in crystal state. In addition, its exceptional AIE effect showed great potential applications in fluorescent thermometer and highly sensitive sensor for selective detection of nitrophenolic compounds. The detection limit for 2,4,6-trinitrophenol was low to 0.168 nM.

1. Introduction

In 2001, Tang et al. found a new class of organic compounds that emitted no or weak fluorescence in solution but had strong emission in aggregation state, and they coined this phenomenon as aggregation-induced emission (AIE) [1]. Since then, AIE compounds have been paid enormously extensive study and are attracting more and more interests because of their colossal application potential in solid emitter and chemo/biosensors [2–10]. It is general knowledge that multiple big substituents (rotors) such as phenyl groups need to be introduced into π-bond plane or aromatic ring (stator) for getting AIE effect. A planar π-conjugation molecule shows AIE effect only when it bears substituents that are not in the same plane while it will display aggregation-caused quenching (ACQ) if it bears no substituent [11–13]. In this way, the AIEgen molecules possess a twisted conformation in which all substituents are not in the same plane due to repulsive force each other [2,8]. The typical examples of AIE compounds include tetraphenylethylene (TPE), hexaphenylsilole, 2-phenylcinnamylnitrile and their derivatives. In solution, the intramolecular motions including rotation of the substituents lead to non-radiative decay of the luminogens. In aggregation state, the intramolecular motion is restricted and, simultaneously, the twisted conformation of the luminogens prevents them from close cofacial π-π stacking that can cause fluorescent quenching. Therefore, the luminogen emits strong fluorescence in aggregation state. This is well-known mechanism of restriction of intramolecular motion (RIM) that has been extensively recognized for AIE phenomena. Multiple substituents and twisted or nonplanar conformation are structural features of one AIEgen compound [2–13].

While AIE compound makes the fluorescence change from off to on or from weak to strong, another class of luminogens with twisted intramolecular charge transfer (TICT) emission mechanism can emit a dual fluorescence and easily adjust the emission colours by change of the environmental conditions [13–15]. This class of luminogen is composed of electron donor (D) and electron acceptor (A) units which easily lead to intramolecular charge transfer (ICT) at the excited state. By combination of AIE and ICT procedure, luminogens can exhibit more advantages both in enhancement of emission intensity and variety of emission colours, which are beneficial for them to be utilized in both solid emitter and sensors [16,17]. In fact, many D-A rotor luminogens are born AIEgens according to RIM mechanism [16–23]. On the other hand, by introducing strong electron-accepting or electron-donating groups into AIE compounds, the AIEgens can display TICT luminescence [24–29]. Due to easy preparation, a large number of D-A AIEgens have been reported recently [16–32]. However, from all the D-A AIEgens, the donor unit and acceptor moiety are connected by single covalent bond and the D-A rotor molecules are in twisted or non-planar conformation just like classical AIE compounds. Here we report that an A-D-A triad, in which donor and acceptor moieties are linked together with carbon-oxygen bonds in fused six-member rings, bears all atoms and substituents in the same plane but displays strong AIE effect. In solution, non-radiation solvent relaxation from hydrogen bonds between solvent and the triad arouses no fluorescence. In aggregation state, due to the repulsive force between multiple oxygen atoms on different molecular planes, highly slipped pi-pi stacking instead of coplanar pi-pi stacking was formed, which leads to the AIE effect. This is a new procedure to AIE phenomenon.

* Corresponding author.
E-mail address: zyansong@hotmail.com (Y.-S. Zheng).

https://doi.org/10.1016/j.dyepig.2019.107556
Received 13 April 2019; Received in revised form 11 May 2019; Accepted 11 May 2019
Available online 15 May 2019
0143-7208/

2. Experimental

2.1. Materials and method

Materials: All reagents and solvents were chemical pure (CP) grade or analytical reagent (AR) grade and were used as received unless otherwise indicated.

Measurements: ^{1}H NMR and ^{13}C NMR spectra were measured on a Bruker AV 400 spectrometer at 298 K. Infrared spectra were recorded on BRUKER EQUINAX55 spectrometer. Absorption spectra were recorded on a Hewlett Packard 8453 UV–Vis spectrophotometer. Mass spectrum was measured on an Ion Spec 4.7 Tesla FTMS instrument. The single crystal data were collected on Rigaku Saturn diffractometer with CCD area detector. All calculations were performed using the SHELXL97 and crystal structure crystallographic software packages. Powder X-ray diffraction (XRD) pattern were measured on a Shimadzu XRD-6000 diffractometer. Fluorescent emission spectra were collected on a Shimadzu RF-5301 fluorophotometer at 298 K. Fluorescence lifetimes were recorded on Edinburgh instruments (FLS 920 spectrometers). Absolute fluorescence quantum yields were recorded on Absolute PL Quantum Yield Spectrometer C11347 with a calibrated integrating sphere system. The fluorescence quantum yield was determined using quinine sulfate ($\Phi_f = 0.546$) in 1 N H_2SO_4 as standard.

Calculation. The geometrical and electronic properties of the triad **3** were performed with the Amsterdam Density Functional (ADF) 2009.01 program package. The calculation was optimized by means of the B3LYP (Becke three parameters hybrid functional with Lee-Yang-Perdew correlation functional) with the 6-31G (d) atomic basis set. Then the electronic structures were calculated at τ-HCTHhyb/6–311 + + G(d,p) level. Molecular orbitals were visualized using ADFview.

2.2. Synthesis of the A-D-A triad 3

Synthesis of tetrahydroxybenzene **2**. To a flask was added 2,5-dihydroxy- [1,4] benzoquinone (1.0 g, 7.15 mmol), concentrated HCl (20 mL). The mixture was constantly stirred with slowly adding to tin powder (1.02 g, 8.58 mmol), refluxed for 1 h. The reaction mixture at 50 °C was filtered off, and the filtrate was cooled at 0 °C to yield white solid. The crude product was recrystallized from THF to yield tetrahydroxybenzene (0.65 g, 65%).

Synthesis of **3**. To a flask was added 2,3,5,6-Tetrafluoro-1,4-benzenedicarbonitrile1(800 mg, 4.0 mmol), tetrahydroxybenzene **2** (280 mg, 2.0 mmol) and potassium carbonate (2.21 g, 16.0 mmol), and DMF (30 mL). The mixture was stirred at room temperature for 2 h. The mixture was filtered and the solvent was removed on a rotary evaporator. The residue was poured into water and was extracted with dichloromethane. After the combined organic phase was dried over anhydrous sodium sulfate and filtered, the filtrate was evaporated to give the crude product, which was recrystallized from DMF to furnish **3** as yellow acicular crystal. After the crystal was stirred to 100 mL diethyl ether solvent to remove DMF and filtered, the filter cake was dried to give pure **3** as yellow solid (813 mg, 88%). Mp > 280 °C; ^{1}H NMR (400 MHz, DMF-d_7) δ 7.42 (s, 2H) ppm. ^{13}C NMR (100 MHz, Acetone-d_6) δ 149.2, 146.4, 142.4, 138.4, 109.4, 107.8; IR (KBr) ν 3060, 2922, 2243, 1649, 1529, 1481, 1412, 1389, 1315, 1266, 1176, 1015, 942, 892, 714, 651 cm^{-1}; HR-MS (ESI$^+$) *m/z* calculated for $C_{22}H_2F_4N_4O_4$ $[M]^+$ 462.0012, found 462.0017 $[M]^+$.

3. Results and discussions

3.1. Synthesis of A-D-A planar triad 3

Tetrafluoroterephthalonitrile **1** is an ideal precursor of acceptor, which can be easily substituted by nitrogen or oxygen atoms to give excellent D-A rotor luminogens [32–34]. When it reacted with 1,2,4,5-tetrahydroxybenzene **2** [35,36] in the presence of potassium carbonate in DMF, A-D-A triad **3**, a derivative of 5,7,12,14-tetraoxapentacene, was obtained in high yield just by recrystallization from DMF (Scheme 1). In this D-A system, the two moieties of donor and acceptor were fused together by double single bonds instead of one single bond.

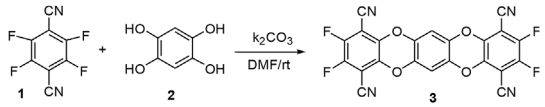

Scheme 1. Synthesis of A-D-A triad **3**.

Table 1
The solubility (mg/mL) and absolute quantum yield (Φ_f) of **3** in different solvent systems.

Solvent System	Φ_f%	mg/mL
solid	24.34	/
toluene	31.61	0.44
benzene	25.24	0.31
chloroform	16.79	0.24
dichloromethane	6.26	0.78
1,2-dichloroethane	2.65	0.26
1,4-dioxane	1.50	0.15
CH_3CN	0.00	0.50
DMSO	0.00	0.28
DMF	0.00	1.97
THF	0.13	0.22
Acetone	0.00	0.83
EA	0.12	0.40
CH_3CH_2OH	0.090	0.11
CH_3OH	0.050	0.012
Hexane	0.00	0.0024
H_2O/DMF 90:10	5.52	/
H_2O/THF 90:10	14.70	/
H_2O/Acetone 50:50	29.13	/

3.2. Photophysical properties of triad 3

Compound **3** was insoluble in hexane and cyclohexane while it had a higher solubility in other conventional solvents such as DMF, acetonitrile, THF, dichloromethane and so on (Table 1). As a yellow-green solid, it showed a main absorption band at about 390 nm in UV–Vis spectrum (Fig. 1A and Fig. S5). But in DMF and DMSO, the absorption maximum wavelength (λ_{max}) for this band is at 395 nm and 398 nm, respectively, which were longer than that in other solvents. In potassium bromide disk, the powder solid had a longer λ_{max} at 415 nm (Fig. 1A).

Compared with absorption spectra, the emission spectra of **3** showed more obvious change not only in solid state but also in solution. While the wet crystals isolated from DMF did not show any fluorescence (Fig. S6), the dry solid powder emitted strong green-yellow light under irradiation of 365 nm light (Fig. 1B–C and Fig. S7). In solution, as the solvent polarity increased, the emission was generally weakened and accompanied by a bathochromic shift. The solution of **3** in benzene (BZ), toluene (TL) and chloroform (TCM) emitted strong blue light, in DCM it had green fluorescence, in 1,2-dichloroethane (DCE) and 1,4-dioxane (DO) a yellow-green fluorescence was observed, and in THF and ethyl acetate (EA) solution it emitted very faint green-yellow light. In contrast, the solution in high polar solvents including acetone (AT), acetonitrile (AN), DMF, DMSO, ethanol, and methanol emitted no any visual fluorescence (Fig. 1D). The emission spectra also confirmed the fluorescence change with the solvents. Besides the fluorescence intensity was generally attenuated with the polarity of the solvent, the emission maximum wavelength λ_{max} was simultaneously increased from 460 nm to 528 nm (Fig. 1E). However, the wavelength increase was not linearly relating to the solvent polarity function (Δf) (Fig. S8) [19,31].

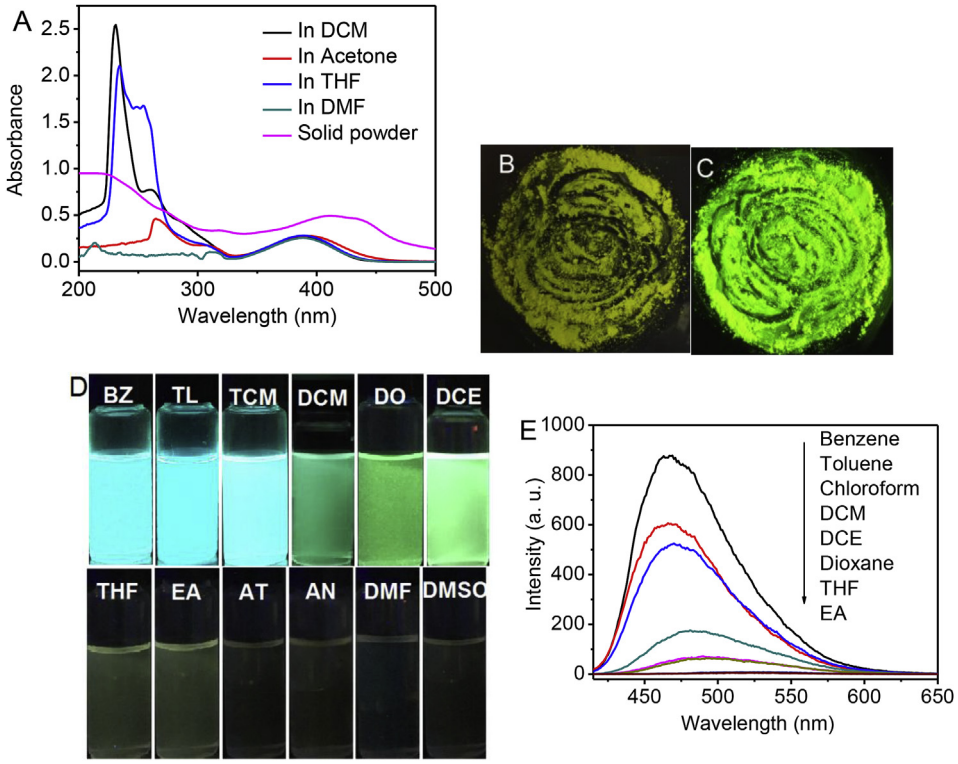

Fig. 1. (A) The absorption spectra of **3** in potassium bromide disk and in partial solvents. (B) Photo of solid powder under daylight. (C, B) Photos of solid powder (C) and solution of **3** in different solvents (D) under a portable 365 nm lamp. (E) The emission spectra of **3** in different solvents. Em/ex slit widths = 3/5, [**3**] = 2×10^{-5} M except methanol and ethanol in which the saturation supernatant of **3** was used.

3.3. AIE phenomenon of the triad 3

Exceptionally, when non-solvent water was added into the solution of **3** in high polar solvents, the solution became strong emissive from no fluorescence. As shown in Fig. 2A, when less than 20% water (volume ratio, the same below) was added into the solution of **3** in DMF, the solution was still clear and non-emissive. By adding more than 20% water, the solution became turbid and started to emit fluorescence. As more water was added and the solution became more turbid, the solution emitted stronger light. At 90% water fraction, the solution emitted brilliant green-yellow light, which was 793 fold stronger than that in pure DMF (Fig. 2B). In addition, besides the major emission band at 520 nm, one minor emission band at 460 nm was also observed. Moreover, while the emission at long wavelength increased, the emission at short wavelength decreased with water, showing a continuous increase of the fluorescence intensity ratio at 520 nm and 460 nm with water fraction. This result indicated that the emission band at long wavelength was ascribed to the intermolecular interaction instead of conformation change of single molecule at the excited state.

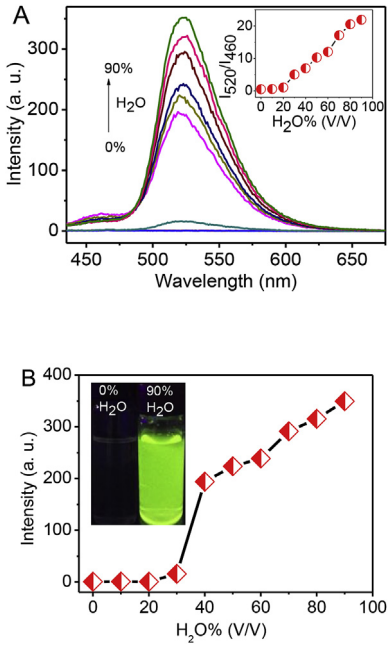

Fig. 2. (A) Change in the emission spectra of **3** in DMF with water fraction. Inset: curve of intensity ratio at 520 nm and 460 nm *vs* water fraction. (B) Curve of fluorescence intensity at 520 nm *vs* water fraction. Inset, photos of solution of **3** in pure DMF and in 90:10 H_2O/DMF under irradiation of a portable 365 nm lamp. λ_{ex} = 409 nm, em/ex slit widths = 3/5, [**3**] = 1×10^{-5} M.

In general, the AIE effect was measured in H_2O/THF solvent system. When water was added into the solution of **3** in THF, the similar phenomenon to the DMF solution was observed (Fig. 3A). At 80% water, the fluorescence intensity got to the largest and increased 103 times more than that in pure THF. When water was increased to 90%, the intensity decreased a little probably due to higher polarity of the mixed solvent and smaller aggregates [19,31]. But it still emitted 71 fold stronger green fluorescence than that in pure THF (Fig. 3B). This change in fluorescence intensity with water fraction was the same as that of some typical AIE molecules [37–39]. Therefore, luminogen **3** could display AIE effect. Meanwhile, a shoulder peak could be made out at short wavelength, showing dual fluorescence just like H_2O/DMF system. Using H_2O/acetone solvent system as test, the fluorescence intensity also had a big increase after water was added, which could get to 100 fold increase at 90% water fraction compared with that in pure acetone (Fig. S9). Simultaneously, obvious dual fluorescence and growth of intensity ratio I_{518}/I_{465} with water were also observed, just like H_2O/DMF and H_2O/THF system.

The measurement of the fluorescence quantum yield further corroborated the conclusion of the AIE effect (Table 1 and Table S1). Measured by integrate sphere, the dry solid powder had 24.3% fluorescence quantum yield. Using quinine sulfate (Φ_f = 0.546) in 1 N H_2SO_4 as standard, the relative fluorescence quantum yield in the three aqueous solvent systems was estimated. In DMF and 90% H_2O/DMF, it was 0% and 4.96%, respectively; In THF and 80% H_2O/THF (intensity

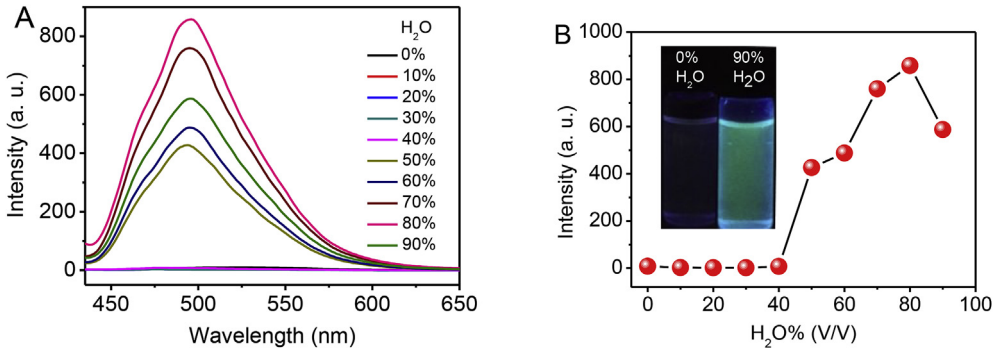

Fig. 3. (A) Change in the emission spectra of **3** with water fraction in THF. (B) Curve of fluorescence intensity *vs* water fraction in acetone. Inset, photos of solution of **3** in pure THF and in 90:10 H_2O/THF under irradiation of a portable 365 nm lamp. λ_{ex} = 416 nm, em/ex slit widths = 5/5, [**3**] = 1×10^{-5} M.

maximum, the same below), it was 0.36% and 16.4%, respectively; In acetone, 50% H_2O/acetone, and 90% H_2O/acetone, it was 0%, 22.0%, and 4.9%, respectively. After aggregation, the fluorescence quantum yield increased very significantly.

3.4. Crystal structure and AIE mechanism of triad 3

Fortunately, single crystal that was suitable for X-ray diffraction was obtained by slow evaporation of the solution of **3** in DMF at room temperature. The crystal structure disclosed that the molecule was composed of five fused six-membered rings, which gave an A-D-A system [40]. The angles between all five six-membered rings were 0.00° and even the fluorine atoms and cyano groups were in the same molecular plane. Therefore, the fluorophore molecule was completely planar (Fig. 4A − 4B). Due to D-A structure, there was a slipped π-π stacking between the donor moiety of one molecule and the acceptor moiety of another one along the long axis of the molecule. However, the π-π stacking area was very small and there was only an edge to edge contact (3.334 Å) between the aromatic rings. The measured pitch angle and roll angle in the slipped π-π stacking were 54.08° and 46.22°, respectively (Fig. S10). The roll angle that was a little larger than 45° confirmed almost no overlapping area between two adjacent molecules [41–43]. However, the short contact was less than the typical π-π stacking distance (3.4 − 3.6 Å) [39] and there were additional interactions (3.350 Å) between electron deficient carbon of cyano groups and centroid of electron-rich tetraoxybenzene rings (Fig. 4C), demonstrating the efficient π-π stacking interaction through edge to edge contact instead of cofacial overlap. Moreover, the slipped π-π stacking could be formed at different slipped π-π stacking directions (Fig. 4D), suggesting the facile availability of the slipped π-π stacking in aggregation state. The different slipped π-π stacking series were bound together by F–C (CN) short contacts (3.091 Å) and interactions between cyano nitrogen and electron-deficient centroid of difluorobenzene ring (3.248 Å). The very small contact area between the molecular planes should be ascribed to the four oxygen atoms bearing two lone electron pairs, which would lead to large repulsive force between oxygen atoms if two molecular planes were cofacially overlapping. Noticeably, more than 1:1 DMF molecules were cocrystallized due to strong hydrogen bond (2.095 Å) between aromatic hydrogen of **3** and carbonyl oxygen atom of DMF (Fig. 4C).

The slipped π-π stacking of the molecular plane should be the reason why the fluorophore emitted dual fluorescence. In nonpolar or less polar solvent, the excited ICT state could not be stabilized by solvation and gave an excited state at high energy level. Therefore, the emission that was like local emission (LE) or monomer emission appeared at short wavelength. Meanwhile, the less solvation attenuated the non-radiative solvent relaxation, which aroused a strong fluorescence. In highly polar solvent, especially in those solvents bearing atom that could form hydrogen bond with the aromatic protons of **3**, the excited ICT state could be stabilized by the solvation. If the

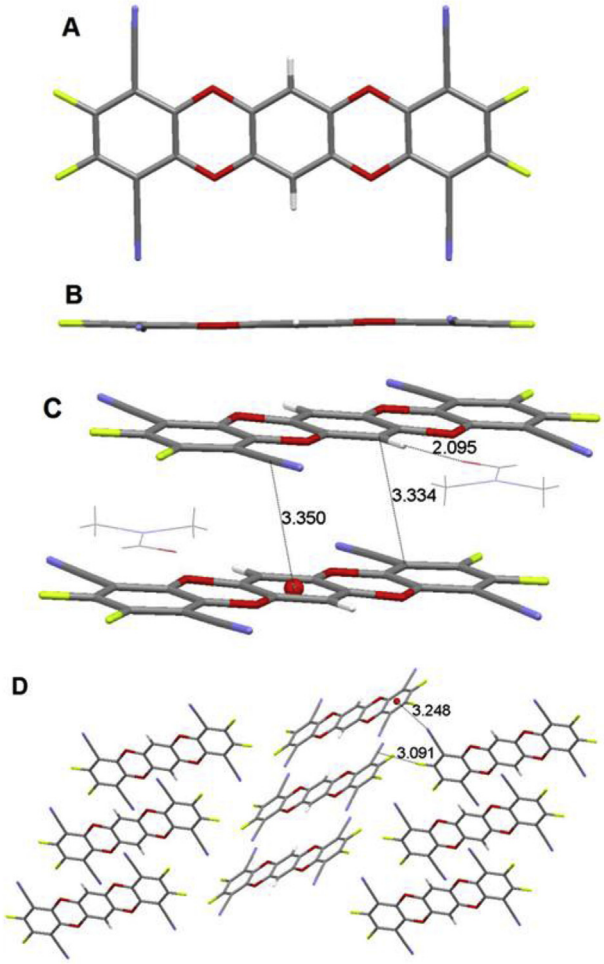

Fig. 4. Crystal structure of **3** viewed (A) perpendicular to the molecular plane and (B) along the molecular plane. (C) The packing of the molecules. (D) The slipped π-π stacking at different directions with the solvent molecules being removed for clarity. The number denotes the intermolecular distance in angstrom and the red ball denotes the centroid of a ring. (For interpretation of the references to colour in this figure legend, the reader is referred to the Web version of this article.)

concentration was higher or in aggregation state, the ICT slipped π-π stacking occurred, which would bring down the energy level of the excited state due to strong Coulomb interactions between ICT states, leading to a bathochromic emission. Meanwhile, due to the strong solvation, the non-radiative solvent relaxation reduced the emission intensity and even caused no any fluorescence. Especially, it should be

mentioned that although THF, 1,4-dioxane and ethyl acetate had less polarity function than that of DCM and DCE, they possessed oxygen atom that could form strong hydrogen bond with the aromatic protons. Therefore, **3** displayed more bathochromic and weaker emission in THF, 1,4-dioxane and EA than in DCM and DCE (Fig. S8). In the case of weak monomer emission or the slipped π-π stacking one that they did not completely overlay each other, dual fluorescence was observed.

The photophysical behaviour of the solid further confirmed this speculation. In wet crystals isolated from DMF solution, no fluorescence was observed under 365 nm light because of cocrytallized DMF molecules that were linked to **3** by hydrogen bonds. After the all DMF molecules were removed, however, the solid emitted strong green-yellow light. By comparing XRD pattern of wet crystals and dry powder, the later kept a good crystal state (Fig. S11). The IR spectrum also had bathochromic shift of about 20 nm compared with the DMF solution, indicating the existence of the slipped π-π stacking. When water was added into the solution, the water could form hydrogen bond with DMF, THF, or acetone etc., and replaced the hydrogen bonds between **3** and the organic solvents (Fig. S6E). The formed aggregates did not involve solvent molecules that could form efficient hydrogen bonds with **3**. Therefore, the formed aggregates by water addition could avoid non-radiative solvent relaxation and make fluorescence increase. In addition, the aggregation could restrict intramolecular motions such as flapping and vibration, which made the emission further increase according to RIM mechanism.

Density functional theory (DFT) analysis suggested that the HOMO orbitals of **3** resided on the tetraoxybenzene unit but not on the cyano groups (Fig. 5). In contrast, the LUMO orbitals localized on the cyano groups but not on the tetraoxybenzene unit both at the ground state and at the excited state. The completely separation of the molecules orbital indicted the ICT process. Meanwhile, at the excited state, the molecular geometry was still planar (Fig. 5B), demonstrating that no bending or twisting occur at the excited state, unlike dihydrobenzophenazine derivatives [44,45]. Therefore, the emission band at long wavelength should come from the aggregation or the slipped π-π stacking instead of TICT process. Furthermore, the bathochromic shift aroused by TICT process was linearly relating to the solvent polarity function, but this emission of **3** was not so [11,19,31]. For A-D-A triad **3**, donor and acceptor moieties were fused through oxygen atoms, which had a stable sp^2 hybridization that led to difficulty of simultaneous rotation of two carbon-oxygen single bonds.

Time-resolved emission decay showed that the fluorescence lifetimes (τ) had an obvious prolonging change from monomer emission to the slipped π-π stacking emission (Fig. S12 and Table S1). The solution in toluene and DCE had 7.05 ns and 1.53 ns fluorescent lifetime, respectively, while the powder solid had 23.8 ns. The lifetime for suspension in 90:10 H_2O/DMF and 80:20 H_2O/THF was 19.4 ns and 56.9 ns, respectively, further indicating longer lifetime of aggregates than monomer. In 50:50 H_2O/acetone, there appeared distinct dual fluorescence, the lifetime was 1.60 ns for the monomer emission at 460 nm and 6.50 ns for the aggregate emission at 520 nm, which was also in accordance with the above observation. This result confirmed the aggregates had stronger fluorescence and longer lifetime.

3.5. Application properties of the triad 3

More interestingly, the A-D-A luminogen displayed emission increase with temperature in 1,2-dichloroethane. When temperature was raised from 0 °C to 80 °C at 10 °C interval each time, the intensity was linearly increased with temperature (Fig. 6A). Meanwhile, the emission maximum wavelength showed hypsochromic shift with temperature. The fatigue resistance for the fluorescence change with temperature was high. By repeatedly heating to 80 °C and then cooling to 25 °C for ten times, the fluorescence spectra and intensity had almost no change (Fig. S13). This result suggested that this fluorophore had a potential for using as thermometer, especially in the conventional temperature

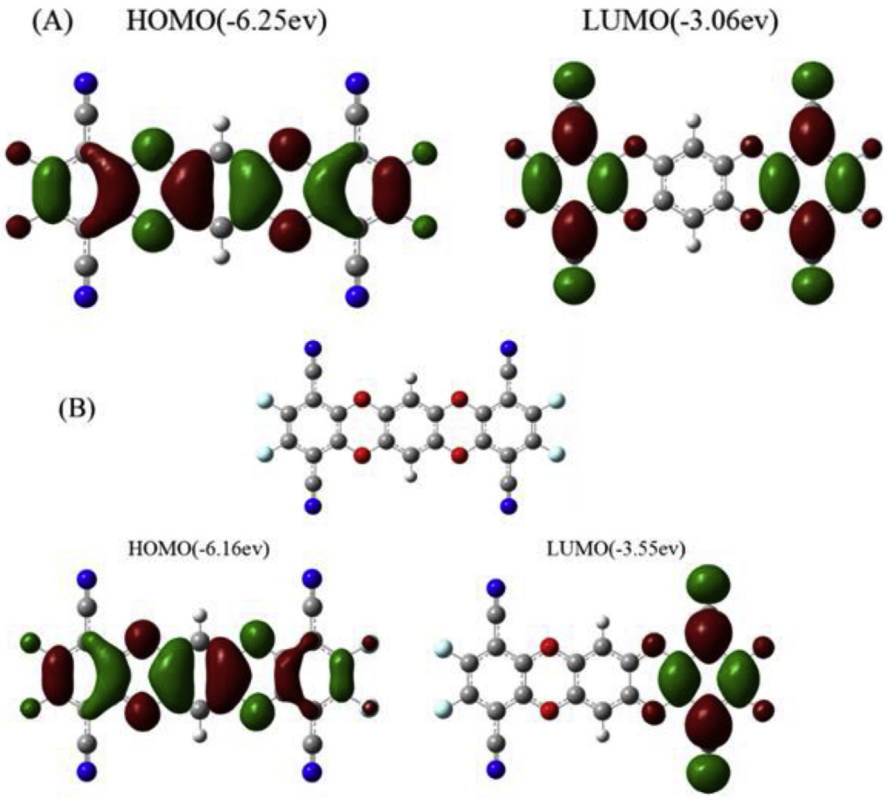

Fig. 5. Frontier molecular orbitals and geometry of **3** calculated by DFT. (A) HOMO and LUMO orbitals at the ground state. (B) Molecular geometry, HOMO and LUMO orbitals at the excited state.

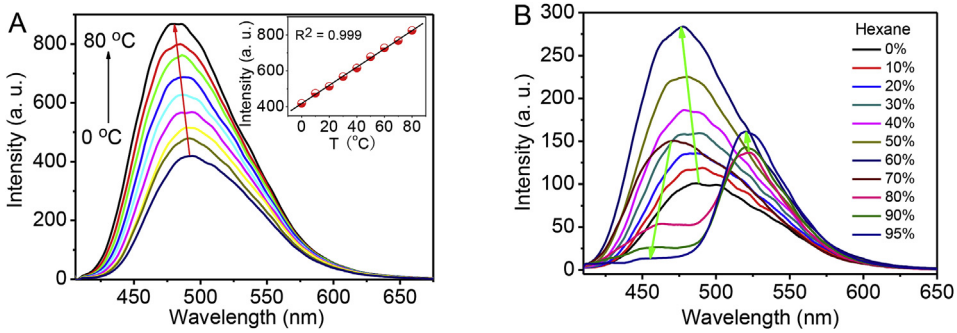

Fig. 6. Change in the emission spectra of **3** in 1,2-dichloroethane with temperature (A) and with hexane fraction (B). The arrows indicating the change tendency of the intensity and emission maximum λ_{max}; inset, linear change of the intensity maximum with temperature. λ_{ex} = 395 nm, [**3**] = 2×10^{-5} M.

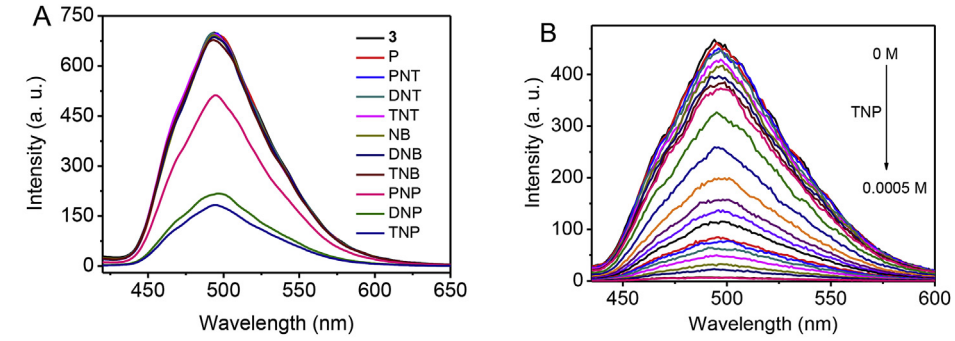

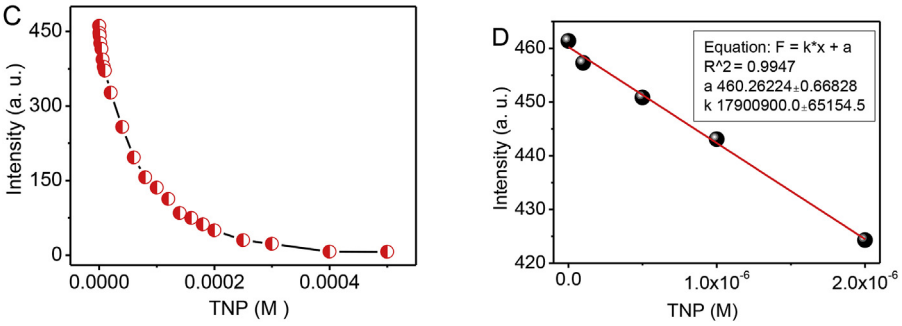

Fig. 7. (A) Fluorescence spectra of **3** in 90:10 H_2O/THF by addition of different NACs. [P] = [PNT] = [DNT] = [TNT] = [NB] = [DNB] = [TNB] = [PNP] = [DNP] = [TNP] = 1.0×10^{-4} M. (B) Change in fluorescence spectra of **3** in 90:10 H_2O/THF with concentration of TNP. (C) Curve of fluorescence intensity at 496 nm *vs.* concentration of TNP from 0 to 5.0×10^{-4} M. (D) Change in fluorescence intensity at 496 nm with concentrations of TNP from 0 to 2.0×10^{-6} M, the red line indicating the fitted one by Origin 7.5 software. [**3**] = 1.0×10^{-5} M λ_{ex} = 416 nm, ex/em slit widths = 5/5 nm. (For interpretation of the references to colour in this figure legend, the reader is referred to the Web version of this article.)

range [13,18,19,29].

The phenomenon of fluorescence increase with temperature may be ascribed to thermal activity or polarity decrease of the solvent. Due to lack of TICT process and the triple state emission, the thermal activity could be excluded. In order to prove the role of the solvent polarity on the fluorescence, the polarity of DCE was continuously lowered by addition of hexane. As expected, when hexane fraction was increased from 0% to 60%, the monomer fluorescence displayed a gradual intensity increase and hypsochromic shift thanks to the polarity decrease (Fig. 6B). When the hexane fraction was got to 70%, **3** started to aggregate and turbid appeared in the solution due to insolubility of **3** in hexane. As the hexane fraction was more than 70% and more aggregation occurred, the monomer emission decreased while the slipped π-π stacking emission increased. This observation not only demonstrated the key reason of fluorescence change with temperature but also further corroborated the AIE effect of **3** even in the pure organic media.

Given that **3** possessed both electron-attracting and electron-donating unit, it should have strong n-π and p-π interactions with nitro aromatic compounds (NACs) both bearing electron-attracting unit and lone-pair electrons of oxygen of nitro groups [46,47]. Moreover, the planar structure will facilitate these interactions due to less steric hindrance. Therefore, with the suspension of **3** in 90:10 H_2O/THF as a sensing system, the effect of NACs on the emission was tested. NACs included 1,3,5-trinitrobenzene (TNB), 2,4,6-trinitrotoluene (TNT), 2,4,6-trinitrophenol (TNP), 1,3-dinitrobenzene (DNB), 2,4-dinitrotoluene (DNT), 2,4-dinitrophenol (DNP), nitrobenzene (NB), *p*-nitrotoluene (PNT), and *p*-nitrophenol (PNP) as well as phenol (P). When the NACs were added to the suspension, respectively, only nitrophenol derivatives obviously alleviated the fluorescence (Fig. S15). Among nitrophenol compounds, TNP showed the largest quenching. This was contrary to other AIE compounds which were more sensitive to TNT rather than TNP [46–49]. The detection limit for TNP was low to 1.68×10^{-7} M (Fig. 7 and Fig. S14).

4. Conclusion

In conclusion, it was found for the first time that a totally planar A-D-A triad could emit strong light in suspension and in solid but no fluorescence in highly polar solvents, displaying a typical AIE effect, although all reported AIE phenomena are based on twisting or non-planar molecules and the planar molecules often usually encounter aggregation-caused quenching problems. In this triad, the repulsive force between oxygen atoms on the different molecular planes prevented the planar molecules from cofacial π-π stacking that could cause quenching. Therefore, the triad showed AIE effect due to RIM process in aggregation state. Considering a large number of fused heterocyclic aromatic compounds, this finding will largely extend the content of AIEgen molecules. More and better AIEgen compounds will be developed from planar aromatic compounds besides twisting molecules.

Acknowledgements

The authors thank National Natural Science Foundation of China (91856125 and 21673089) and HUST Graduate Innovation Fund for financial support, and thank the Analytical and Testing Centre at Huazhong University of Science and Technology for measurement.

Appendix A. Supplementary data

Supplementary data related to this article can be found at https://doi.org/10.1016/j.dyepig.2019.107556.

References

[1] Luo J-D, Xie Z-L, Lam JWY, Cheng L, Chen H-Y, Qiu C-F, Kwok HS, Zhan X-W, Liu Y-Q, Zhu D-B, Tang B-Z. Aggregation-induced emission of 1-methyl-1, 2, 3, 4, 5-pentaphenylsilole. Chem Commun 2001(18):1740–1.
[2] Mei J, Leung NLC, Kwok RTK, Lam JWY, Tang B-Z. Aggregation-induced emission: together we shine, united we soar!. Chem Rev 2015;115(21):11718–940.
[3] Feng H-T, Yuan Y-X, Xiong J-B, Zheng Y-S, Tang B-Z. Macrocycles and cages based on tetraphenylethylene with aggregation-induced emission effect. Chem Soc Rev 2018;47(19):7452–76.
[4] Xiong J-B, Xie W-Z, Sun J-P, Wang J-H, Zhu Z-H, Feng H-T, Guo D, Zhang H, Zheng Y-S. Enantioselective recognition for many different kinds of chiral guests by one chiral receptor based on tetraphenylethylene cyclohexylbisurea. J Org Chem 2016;81(9):3720–6.
[5] Shi J, Li Y, Li Q-Q, Li Z. Enzyme-responsive bioprobes based on the mechanism of aggregation-induced emission. ACS Appl Mater Interfaces 2017;10(15):12278–94.
[6] Feng G, Liu B. Aggregation-induced emission (AIE) dots: emerging theranostic nanolights. Acc Chem Res 2018;51(6):1404–14.
[7] Ma L, Feng X, Wang S, Wang B. Recent advances in AIEgen-based luminescent metal–organic frameworks and covalent organic frameworks. Mater Chem Front 2017;1(12):2474–86.
[8] Hong Y, Lam JWY, Tang B-Z. Aggregation-induced emission. Chem Soc Rev 2011;40(11):5361–88.
[9] Xiong J-B, Yuan Y-X, Wang L, Sun J-P, Qiao W-G, Zhang H-C, Zheng Y-S. Evidence for aggregation-induced emission from free rotation restriction of double bond at excited state. Org Lett 2018;20(2):373–6.
[10] Xiong J-B, Feng H-T, Sun J-P, Xie W-Z, Yang D, Liu M-H, Zheng Y-S. The fixed propeller-like conformation of tetraphenylethylene that reveals aggregation-induced emission effect, chiral recognition, and enhanced chiroptical property. J Am Chem Soc 2016;138(36):11469–72.
[11] Yang L, Ye P, Li W, Zhang W, Guan Q, Ye C, Peng Q. Uncommon aggregation-induced emission molecular materials with highly planar conformations. Adv Optical Mater 2018;6(9):1701394.
[12] Zheng Y-S, Hu Y-J. Chiral recognition based on enantioselectively aggregation-induced emission. J Org Chem 2009;74(15):5660–3.
[13] Li D-M, Zheng Y-S. Highly enantioselective recognition of a wide range of carboxylic acids based on enantioselectively aggregation-induced emission. Chem Commun 2011;47(36):10139–41.
[14] Grabowski ZR, Rotkiewicz K, Rettig W. Structural changes accompanying intramolecular electron transfer: focus on twisted intramolecular charge-transfer states and structures. Chem Rev 2003;103(10):3899. -4032.
[15] Yang Z, Cao J, He Y, Yang J-H, Kim T, Peng X, Kim JS. Macro-/micro-environment-sensitive chemosensing and biological imaging. Chem Soc Rev 2014;43(13):4563–601.
[16] Wang X, Wolfbeis OS, Meier RJ. Luminescent probes and sensors for temperature. Chem Soc Rev 2013;42(19):7834–69.
[17] Liese D, Haberhauer G. Rotations in excited ICT states–fluorescence and its microenvironmental sensitivity. Isr J Chem 2018;58(8):813–26.
[18] Sasaki S, Drummen GPC, Konishi G. Recent advances in twisted intramolecular charge transfer (TICT) fluorescence and related phenomena in materials chemistry. J Mater Chem C 2016;4(14):2731–43.
[19] Hu R, Lager E, Aguilar-Aguilar A, Liu J, Lam JW, Sung HH, Tang B-Z. Twisted intramolecular charge transfer and aggregation-induced emission of BODIPY derivatives. J Phys Chem C 2009;113(36):15845–53.
[20] Cao C, Liu X, Qiao Q, Zhao M, Yin W, Mao D, Xu Z. A twisted-intramolecular-charge-transfer (TICT) based ratiometric fluorescent thermometer with a mega-Stokes shift and a positive temperature coefficient. Chem Commun 2014;50(99):15811–4.
[21] Hariharan PS, Venkataramanan NS, Moon D, Anthony SP. Self-reversible mechanochromism and thermochromism of a triphenylamine-based molecule: tunable fluorescence and nanofabrication studies. J Phys Chem C 2015;119(17):9460–9.
[22] Sasaki S, Suzuki S, Sameera WMC, Igawa K, Morokuma K, Konishi GI. Highly twisted N, N-dialkylamines as a design strategy to tune simple aromatic hydrocarbons as steric environment-sensitive fluorophores. J Am Chem Soc 2016;138(26):8194–206.
[23] Peng Z, Ji Y, Huang Z, Tong B, Shi J, Dong Y. A strategy for the molecular design of aggregation-induced emission units further modified by substituents. Mater Chem Front 2018;2(6):1175–83.
[24] Cheng Y, Wang J, Qiu Z, Zheng X, Leung NL, Lam JW, Tang B-Z. Multiscale humidity visualization by environmentally sensitive fluorescent molecular rotors. Adv Mater 2017;29(46):1703900.
[25] Gao H, Xu D, Wang Y, Wang Y, Liu X, Han A, Zhang C. Effects of alkyl chain length on aggregation-induced emission, self-assembly and mechanofluorochromism of tetraphenylethene modified multifunctional β-diketonate boron complexes. Dyes Pigments 2018;150:59–66.
[26] Li J, Yang C, Peng X, Chen Y, Qi Q, Luo X, Lai W-Y, Huang W. Stimuli-responsive solid-state emission from o-carborane–tetraphenylethene dyads induced by twisted intramolecular charge transfer in the crystalline state. J Mater Chem C 2018;6(1):19–28.
[27] Zhao Y, He S, Yang J, Sun H, Shen X, Han X, Ni Z. Study on TICT emission of TPE-BODIPY derivatives mediated by methyl group on BODIPY. Opt Mater 2018;81:102–8.
[28] Sun H, Tang X-X, Miao B-X, Yang Y, Ni Z. A new AIE and TICT-active tetraphenylethene-based thiazole compound: synthesis, structure, photophysical properties and application for water detection in organic solvents. Sens Actuators, B 2018;267:448–56.
[29] Feng H-T, Xiong J-B, Zheng Y-S, Pan B, Zhang C, Wang L, Xie Y. Multicolor emissions by the synergism of intra/intermolecular slipped π–π stackings of tetraphenylethylene-DiBODIPY conjugate. Chem Mater 2015;27(22):7812–9.
[30] Naito H, Nishino K, Morisaki Y, Tanaka K, Chujo Y. Solid-state emission of the anthracene-o-carborane dyad from the twisted-intramolecular charge transfer in the crystalline state. Angew Chem Int Ed 2017;56(1):254–9.
[31] Li K, Liu Y, Li Y, Feng Q, Hou H, Tang B-Z. 2, 5-bis (4-alkoxycarbonylphenyl)-1, 4-diaryl-1, 4-dihydropyrrolo [3, 2-b] pyrrole (AAPP) AIEgens: tunable RIR and TICT characteristics and their multifunctional applications. Chem Sci 2017;8(10):7258–67.
[32] Song F, Xu Z, Zhang Q, Zhao Z, Zhang H, Sung HHY, Williams ID, Lam JWY, Qin A, Ma D, Tang B-Z. Highly efficient circularly polarized electroluminescence from aggregation-induced emission luminogens with amplified chirality and delayed fluorescence. Adv Funct Mater 2018;28(17):1800051.
[33] Feuillastre S, Pauton M, Gao L, Desmarchelier A, Riives AJ, Prim D, Tondelier D, Geffroy B, Muller G, Clavier G, Pieters G. Design and synthesis of new circularly polarized thermally activated delayed fluorescence emitters. J Am Chem Soc 2016;138(12):3990–3.
[34] Uoyama H, Goushi K, Shizu K, Nomura H, Adachi C. Highly efficient organic light-emitting diodes from delayed fluorescence. Nature 2012;492(7428):234–8.
[35] Dempsey JM, Zhang Q-W, Oliver AG, Smith BD. New tetralactam hosts for squaraine dyes [J]. Org Biomol Chem 2018;16(46):8976–83.
[36] Mills SJ, Vandeput F, Trusselle MN, Safrany ST, Erneux C, Potter BVL. Benzene polyphosphates as tools for cell signalling: inhibition of inositol 1, 4, 5-trisphosphate 5-phosphatase and interaction with the PH domain of protein kinase Bα[J]. Chembiochem 2008;9(11):1757–66.
[37] Shen X-Y, Wang Y-J, Zhao E, Yuan W-Z, Liu Y, Lu P, Qin A, Ma Y, Sun J-Z, Tang B-Z. Effects of substitution with donor–acceptor groups on the properties of tetraphenylethene trimer: aggregation-induced emission, solvatochromism, and mechanochromism. J Phys Chem C 2013;117(14):7334–47.
[38] Huang J, Tang R, Zhang T, Li Q, Yu G, Xie S, Liu Y, Ye S, Qin J, Li Z. A new approach to prepare efficient blue AIE emitters for undoped OLEDs. Chem Eur J 2014;20(18):5317–26.
[39] Feng H-T, Zheng Y-S. Highly sensitive and selective detection of nitrophenolic explosives by using nanospheres of a tetraphenylethylene macrocycle displaying aggregation-induced emission. Chem Eur J 2014;20(1):195–201.
[40] The crystallographic data of **3** have been deposited in the Cambridge Structural Database as CCDC 1853488.
[41] Curtis MD, Cao J, Kampf JW. Solid-state packing of conjugated oligomers: from π-stacks to the herringbone structure. J Am Chem Soc 2004;126(13):4318–28.
[42] Yoon SJ, Chung JW, Gierschner J, Kim KS, Choi MG, Kim D, Park SY. Multistimuli two-color luminescence switching via different slip-stacking of highly fluorescent molecular sheets. J Am Chem Soc 2010;132(39):13675–83.
[43] Galer P, Korošec RC, Vidmar M, Šket B. Crystal structures and emission properties of the BF2 complex 1-phenyl-3-(3, 5-dimethoxyphenyl)-propane-1, 3-dione: multiple chromisms, aggregation-or crystallization-induced emission, and the self-assembly effect. J Am Chem Soc 2014;1136(20):7383–94.
[44] Zhang Z, Wu Y-S, Tang K-C, Chen C-L, Ho JW, Su J, Tian H, Chou P-T. Excited-state

conformational/electronic responses of saddle-shaped N, N′-disubstituted-dihydrodibenzo [a, c] phenazines: wide-tuning emission from red to deep blue and white light combination. J Am Chem Soc 2015;137(26):8509–20.
[45] Humeniuk HV, Rosspeintner A, Licari G, Kilin V, Bonacina L, Vauthey E, Sakai N, Matile S. White-fluorescent dual-emission mechanosensitive membrane probes that function by bending rather than twisting. Angew Chem Int Ed 2018;130(33):10719–23.
[46] Xiong J-B, Wang J-H, Li B, Zhang C, Tan B, Zheng Y-S. Porous interdigitation molecular cage from tetraphenylethylene trimeric macrocycles that showed highly selective adsorption of CO2 and TNT vapor in air. Org Lett 2018;20(2):321–4.
[47] Feng H-T, Wang J-H, Zheng Y-S. CH3–π interaction of explosives with cavity of a TPE macrocycle: the key cause for highly selective detection of TNT[J]. ACS Appl Mater Interfaces 2014;6(22):20067–74.
[48] Wang J-H, Feng H-T, Zheng Y-S. Synthesis of tetraphenylethylene pillar [6] arenes and the selective fast quenching of their AIE fluorescence by TNT[J]. Chem Commun 2014;50(77):11407–10.
[49] Xiong J-B, Feng H-T, Wang J-H, Zhang C, Li B, Zheng Y-S. Tetraphenylethylene foldamers with double hairpin-turn linkers, TNT-binding mode and detection of highly diluted TNT vapor. Chem Eur J 2018;24(8):2004–12.